Available online at www.sciencedirect.com
ScienceDirect
Trans. Nonferrous Met. Soc. China 34(2024) 3233−3250

Transactions of
Nonferrous Metals
Society of China
www.tnmsc.cn

Effects of cold rolling path on recrystallization behavior and mechanical properties of pure copper during annealing

Jing CHEN[1,2,3], Wen-jie XU[1,2], Jia-hao YANG[1,2], Zhi YANG[1], Hong-li SHI[1,2],
Gao-yong LIN[3], Zhu-min LI[1,2], Xu SHEN[4], Bo JIANG[5], Hui-qun LIU[3], Kai-xuan GUI[1,2]

1. School of Materials Science and Engineering, Anhui Polytechnic University, Wuhu 241000, China;
2. Anhui Key Laboratory of High-Performance Non-ferrous Metal Materials,
Anhui Polytechnic University, Wuhu 241000, China;
3. School of Materials Science and Engineering, Central South University, Changsha 410083, China;
4. Institute of Plasma Physics, Chinese Academy of Sciences, Hefei 230031, China;
5. School of Materials Science and Engineering, Changzhou University, Changzhou 213164, China

Received 3 July 2024; accepted 19 September 2024

Abstract: The recrystallization behavior, grain boundary characteristic distribution, and mechanical properties of pure Cu sheets that were subjected to different cold rolling paths, and then annealed at 400 °C for 10, 30, 60, and 420 min, were investigated. Different rolling paths changed the grain boundary orientations of cold-rolled copper, causing recrystallized grains to nucleate and grow in an oriented manner. However, the evolution of the texture indicated that cold-rolled copper with different rolling paths did not show an obvious preferred orientation after annealing. The RD-60 specimen exhibited the smallest grain size (6.6 μm). The results indicated that the grain size and low-Σ CSL grain boundaries worked together to provide RD-60 samples with appropriate mechanical properties and high plasticity. The yield strength, ultimate tensile strength, and elongation of RD-60 sample were 81 MPa, 230 MPa, and 49%, respectively. These results could provide guidance for tuning the microstructures and properties of pure Cu foils, as well as designing fabrication routes for pure Cu foils through processes such as rolling and drawing.

Key words: rolling path; grain boundary characteristic distribution; pure copper; mechanical properties

1 Introduction

Pure Cu and Cu alloys are ideal materials for use in power transmission equipment, flexible circuit boards, and transformers owing to their remarkable ductility, bending resistance, and conductivity [1−3]. With the rapid growth of electronic information technology, particularly in the 5G era, social Internet products have begun to develop into thin, light, and compact devices; rolled copper foil is particularly advantageous in these devices, and as a result, its use has consistently increased [4,5]. Indeed, rolled copper foil exhibits superior strength and lower surface roughness, making it increasingly useful in the high-end electronics industry [6,7]. The key technologies for the fabrication of copper components include the application of mechanical deformation and subsequent heat treatment [8−10].

Rolling is a thermomechanical deformation process that can improve the strength of pure Cu through grain refinement and strain hardening. The applied rolling path has a significant influence on

---

Corresponding author: Hui-qun LIU, Tel: +86-13975809193, E-mail: liuhuiqun@csu.edu.cn;
Kai-xuan GUI, Tel: +86-13909636725, E-mail: guikx@ahpu.edu.cn

DOI: 10.1016/S1003-6326(24)66605-7

the microstructure, dislocation arrangement, texture, and recrystallization kinetics of the rolled material [11−13]. Conventional unidirectional rolling, which is frequently used to mechanically deform plate or sheet products, typically results in an anisotropic texture and microstructure or gradients throughout the material thickness. Therefore, many different rolling procedures, including cross rolling and asymmetric rolling, have been developed to improve microstructural homogeneity. In cold-rolled pure Cu, the rolling path can affect the strain-hardening rate and grain size distribution, in turn influencing its recrystallization behavior and microstructural evolution [14,15]. GUPTA et al [16] investigated the evolution of the deformed and statically recrystallized microstructures in room-temperature cross-rolled Cu, and LI et al [17,18] manufactured Cu foil with improved bending properties using a double-cross-rolling process. In addition, DENG et al [19] determined textural evolution of pure Ta under different rolling paths, OERTEL et al [20] utilized cross rolling to increase the γ-fiber texture of Mo plates and thereby improved the formability, and XU et al [21,22] tailored the microstructure and properties of dual-phase Mg−8Li and Cu−Fe alloys by varying the applied rolling paths. These rolling methods can also be applied to pure Cu sheets.

Notably, special grain boundaries serve as key material enhancers by suppressing the dislocation motion and electron scattering at twin boundaries while increasing the hardness and conductivity. Therefore, the grain boundary characteristics and grain sizes within pure Cu must be controlled to achieve the required performance. Numerous studies have reported that the grain boundary characteristic distribution (GBCD) can significantly affect the mechanical and physical properties of metallic materials, and can be optimized through thermomechanical processing techniques to improve service performance [23−25]. For example, ZHU et al [26] introduced cryogenic deformation to tailor the dislocation accumulation mode and modify the GBCD of Incoloy 925, YOU et al [27] investigated the GBCD and deformation behavior of a transformation-induced plasticity-assisted high-entropy alloy, and YANG et al [23] studied the evolution of low-strain grain boundaries owing to strain-induced boundary migration in pure Cu. The results of previous grain boundary studies indicate that the numerous new Σ3 boundaries generated behind the migrating grain boundary front increase the proportion of special boundaries and that introducing low-energy segments disrupts the connectivity of random high-angle boundary networks [28,29].

The Cu foil may demonstrate a preferred orientation during the rolling process, resulting in hardness and anisotropy. Furthermore, the tensile plasticity of Cu foil may be affected by the applied rolling process. Finally, the grain recrystallization and grain growth that occur during annealing can have different effects on the recrystallization behavior, characteristic grain boundary distribution, and mechanical properties of Cu foil according to the applied rolling process. However, during the manufacturing of rolled copper foil, improperly set control parameters can result in infrequent deformation instability and wrinkling when the rolling deformation reaches approximately 20 μm. This makes it difficult to continue the deformation process to reduce the thickness of the rolled copper foil. Therefore, to better understand the microstructural and textural changes that occur during the rolling and annealing processes and ultimately optimize the manufacturing of Cu foil, the recrystallization behavior, characteristic grain boundary distribution, and mechanical properties of cold-rolled Cu according to the applied rolling path and annealing time were investigated this study.

2 Experimental

2.1 Material

The 1.0 mm-thick rolled TP2 Cu sheets employed as raw materials are denoted as the "as-received material". The optical micrograph of this material shown in Fig. 1(a) depicts its metallographic structures at low magnification; the enlarged view in Fig. 1(b) shows that its morphology was composed of equiaxed grains and annealing twins with an average size of ~18 μm.

2.2 Specimen fabrication

The as-received material sheets were cold-rolled to 0.5 mm (50% rolling reduction) at room temperature using three different rolling paths shown schematically in Fig. 2: the rolling direction (RD), transverse direction (TD), and cross rolling

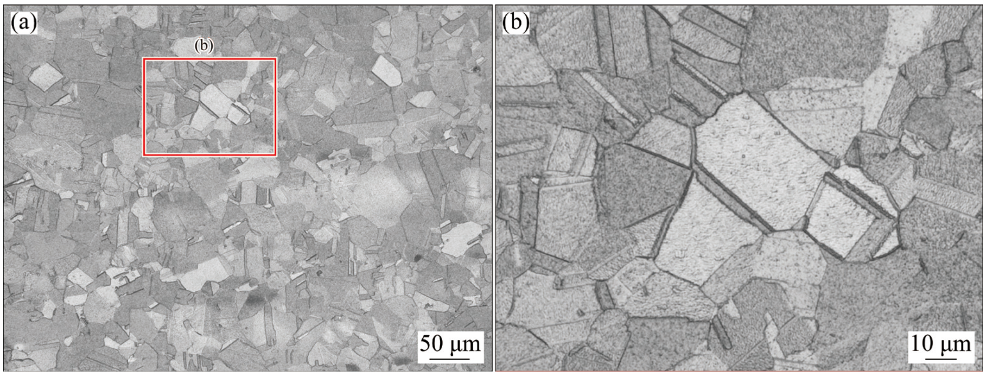

Fig. 1 Optically observed microstructure of initial materials

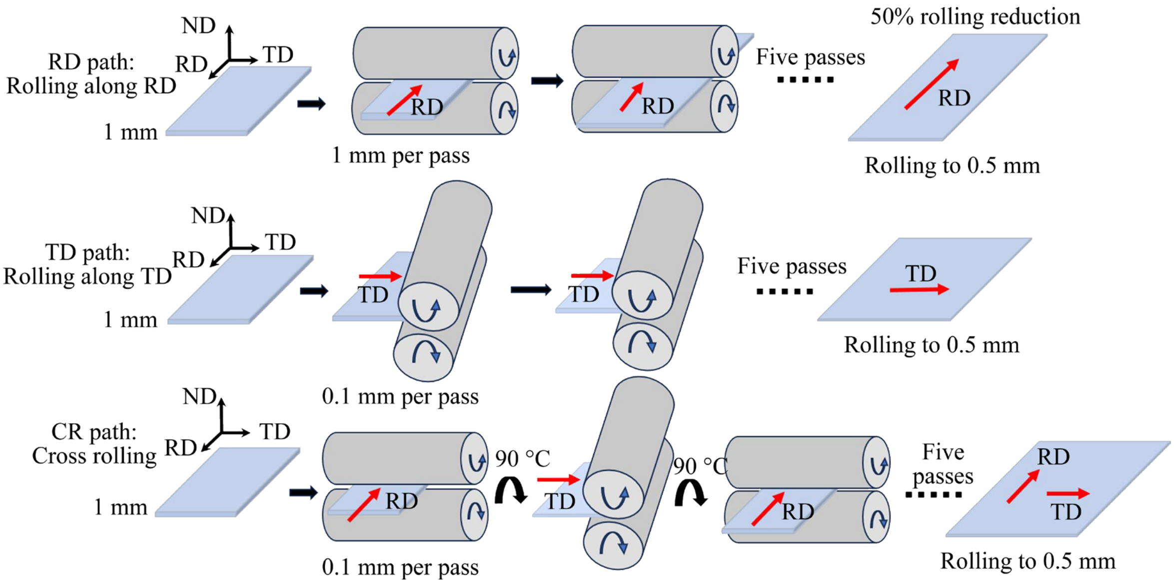

Fig. 2 Schematic diagrams of rolling paths considered in this study

(CR) paths. Thus, the RD, TD, and CR specimens were respectively subjected to multiple rolling passes parallel, perpendicular, and alternating between parallel and perpendicular to the rolling direction applied to fabricate the as-received material sheet. The extent of compression per pass was about 0.1 mm, and after approximately five passes of rolling deformation, the sheet was deformed from a thickness of 1.0 to 0.5 mm. To study the effect of rolling path on recrystallization behaviors, GBCDs, and mechanical properties of the pure copper, the cold-rolled specimens were subsequently annealed at 400 °C for 10, 30, 60, 180, and 420 min, and then immediately quenched in water to room temperature. The specimen nomenclature accordingly expresses the rolling direction and annealing time; for example, the specimen cold-rolled along the as-received rolling direction and annealed at 400 °C for 60 min is represented as RD-60.

2.3 Characterization methods

The microstructure of each specimen was characterized using optical microscopy. Prior to characterization, each specimen was ground, polished, and etched in a solution of $FeCl_3$ + HCl + methanal for 25 s. The microstructural evolution and GBCD were further investigated via scanning electron microscope−electron backscatter diffraction (SEM-EBSD) using a TESCAN CLARA SEM equipped with an Oxford EBSD acquisition camera (NordlysMax3). To characterize the surface texture of each specimen, it was first mechanically polished with wet 3000 grit silicon carbide sandpaper, polished with 1 μm diamond grinding paste, and then electropolished with a solution of 80 mL phosphoric acid and 100 mL ethanol at room temperature under a voltage of 20 V for 35 s approximately. The EBSD patterns were acquired at an acceleration voltage of 20 kV, using the RD−TD plane with a step size of 0.6 μm. The area captured by each image was 200 μm × 200 μm, and the measurement results were analyzed using the Channel 5 software.

Tensile test specimens with gauge dimensions of 15 mm × 4 mm × 0.5 mm were cut from each sheet along the as-received rolling direction. Uniaxial tensile tests were performed on these specimens by an AGS-X100KN instrument at room temperature using a displacement-based tension loading rate of 1 mm/min. A strain extensometer was employed to ensure the collection of accurate stress–strain data.

3 Results and discussion

3.1 Effect of rolling paths on microstructure

The optical microstructures of the cold-rolled RD, TD, and CR specimens are shown in Fig. 3, which indicates that the grains in each specimen were elongated along the deformation direction to form a typical deformation microstructure. As shown, the microstructures of the CR-rolled samples tended to an equiaxed morphology. Additionally, twins can be observed in the deformation microstructure, as indicated by the positions marked with red arrows. Their deformation behaviors varied according to the applied rolling path, forming deformed structures with different morphologies.

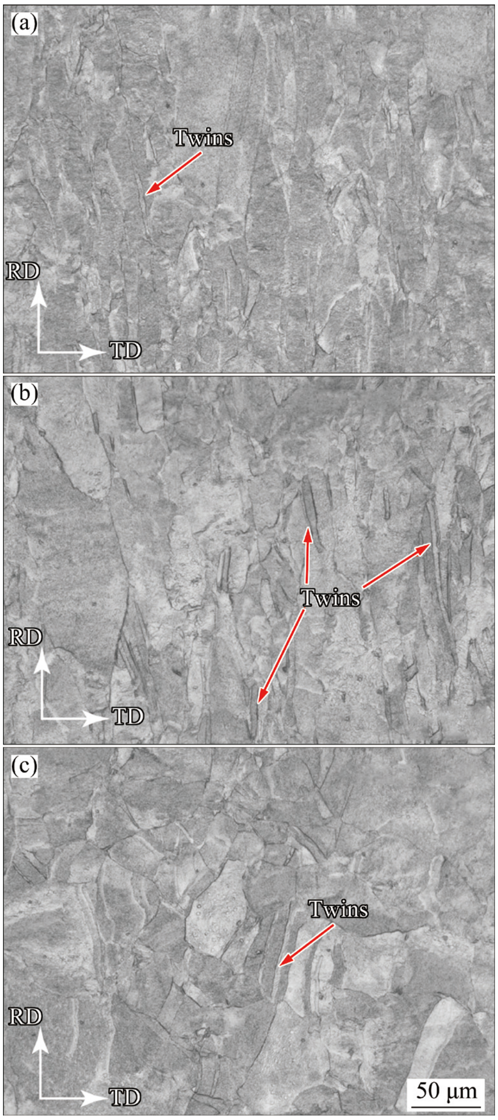

Fig. 3 Optical micrographs of Cu specimens after cold rolling with different rolling paths: (a) RD; (b) TD; (c) CR

3.2 Recrystallization behavior during annealing

The change in the Vickers hardness of the cold-rolled Cu specimens with different rolling paths annealed at 400 °C for different durations is shown in Fig. 4. The cold-rolled samples with different rolling paths during annealing had similar Vickers hardness evolution. After annealing for 10 min, the Vickers hardness of the specimens decreased dramatically from ~140 HV to ~70 HV, indicating that the samples underwent recovery and recrystallization. After annealing for 30 min, the hardness of each specimen decreased more slowly to ~62 HV and declined even more slowly thereafter to ~60 HV and ~58 HV after 60 and 180 min, respectively, indicating that the cold-rolled Cu had essentially completed the recrystallization process. Finally, the Vickers hardness of each specimen decreased slightly again after annealing for 420 min, indicating that the recrystallized grains exhibited grain growth after long-term annealing. These results suggest that the ideal recrystallization condition for the cold-rolled pure Cu specimens was annealing at 400 °C for 60 min, regardless of the rolling path.

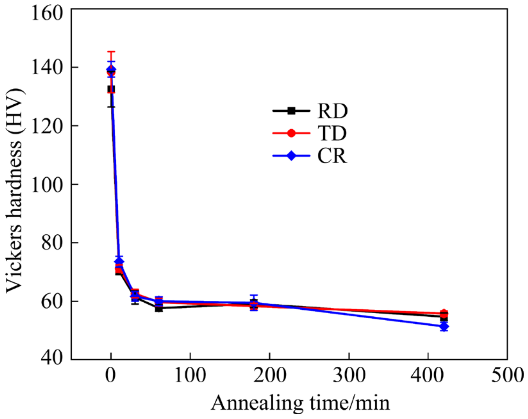

Fig. 4 Variation of Vickers hardness of pure Cu sheets annealed at 400 °C for different durations

To characterize the microstructural evolutions during annealing, optical micrographs of the cold-rolled specimens subjected to different annealing times are shown in Fig. 5. After annealing for 10 min, small, recrystallized nuclei were formed, and the elongated deformed grains were basically invisible, as shown in Fig. 5(a). The red arrows indicate the deformed microstructure, while the white arrow indicates the recrystallized nuclei. These results indicated that recovery and recrystallization occurred in the RD-10 specimen. As shown in Fig. 5(b), the TD-10 sample still maintained elongated deformed grains, as indicated by the red arrows, indicating that the sample mainly underwent the recovery. This is because different rolling paths alter the deformation storage energy and grain boundary characteristics of the material, therefore increasing the recrystallization temperature. After annealing for 10 min, elongated grains can still be observed in the TD-10 sample, while elongated deformed grains of the RD-10 sample are almost invisible. There are some recrystallized nuclei also formed in deformation and distortion areas. In Specimen CR-10, the recrystallized nuclei were preferentially formed in areas with large local energy storage and deformed structures were observed, as shown in Fig. 5(c).

After annealing for 30 min, fine recrystallized grains were formed, but small portions of the deformed microstructure remained, as shown in Figs. 5(d−f). During annealing, the recrystallized nuclei grow by absorbing the energy stored in the

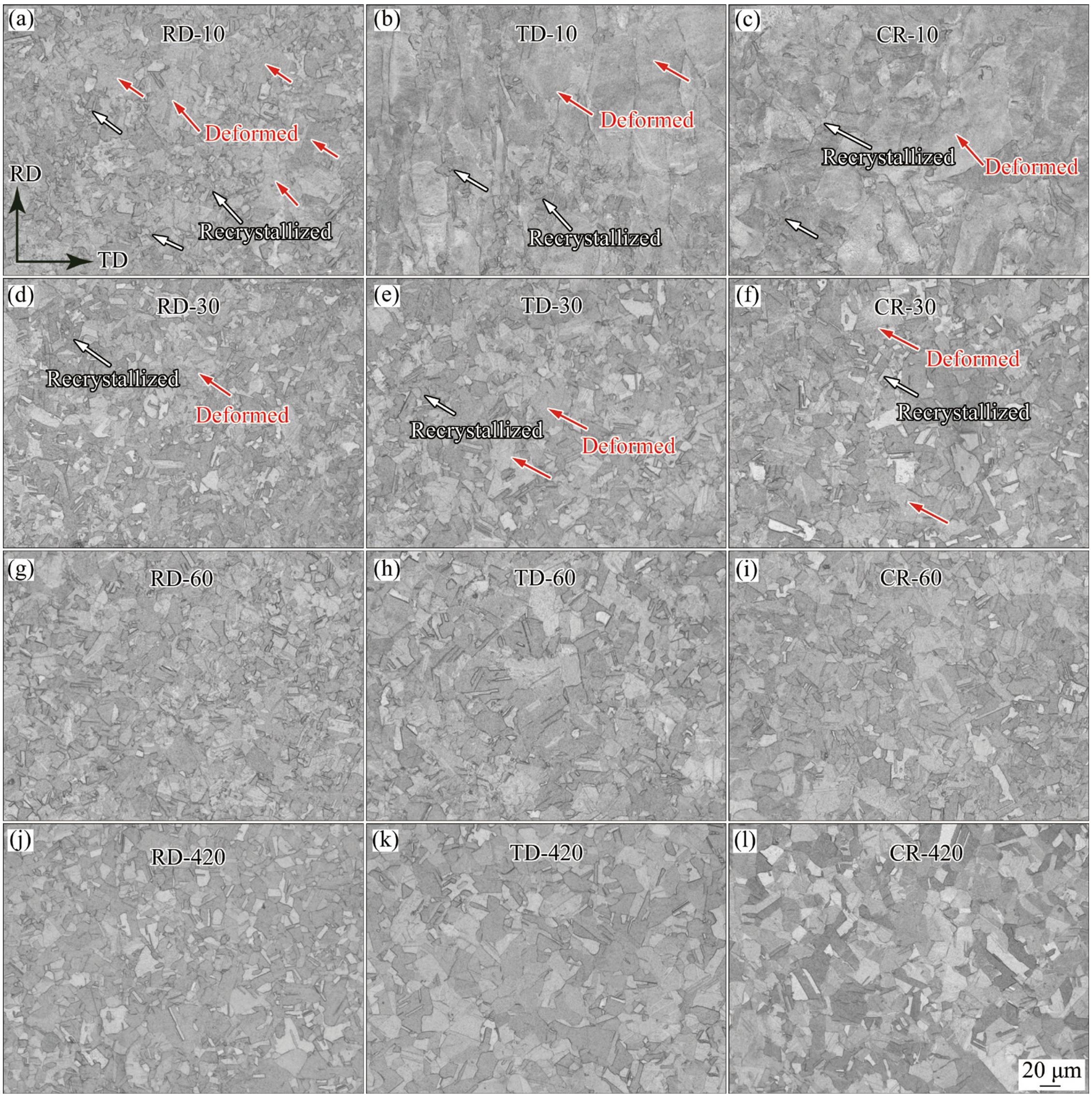

Fig. 5 Optical micrographs of cold-rolled copper with different rolling paths annealed at 400 °C for different durations: (a−c) 10 min; (d−f) 30 min; (g−i) 60 min; (j−l) 420 min

distorted microstructure via atomic diffusion. However, owing to the short annealing time, the recrystallized nuclei did not grow, forming small recrystallized grains while maintaining a slightly distorted microstructure.

After annealing for 60 min, fine recrystallized grains gradually expanded through grain boundary migration, creating smaller recrystallized grains, as shown in Figs. 5(g−i). At locations with significant distortion, a core of new undistorted grains were formed, which gradually consumed the surrounding deformed matrix and grew until each deformed structure was entirely reformed into new undistorted fine equiaxed grains. Finally, after annealing for 420 min, the recrystallized grain size stabilized, as shown in Figs. 5(j−l). As shown in Figs. 4 and 5, the evolution of the microstructure during annealing was congruent with the change in the Vickers hardness.

Based on the observed changes in the microstructures of the specimens with annealing time, four different recrystallization stages (0, 10, 60, and 420 min) were selected to study the recrystallization behaviors and texture evolutions of the specimens using EBSD. Figures 6(a−c) show the EBSD orientation maps of the cold-rolled RD, TD, and CR specimens, respectively, in which deformed grains with ⟨100⟩ and ⟨111⟩ orientations can be observed along the normal direction (ND) of all specimens. The orientation maps of the specimens after annealing for 10 min are shown in Figs. 6(d−f), which indicate that each specimen underwent recovery and recrystallization at high-distortion-energy locations, forming fine recrystallized nuclei. However, owing to the short annealing time, the deformed structures were still present. Relatively elongated grains were also observed along the direction of rolling deformation for each specimen. The texture primarily reflected ⟨100⟩//ND grains, indicating several deformed ⟨111⟩//ND grains that turned into ⟨001⟩//ND grains after annealing for 10 min.

The EBSD orientation maps of the RD-60, TD-60, and CR-60 specimens are shown in Figs. 6(g−i), respectively, indicating that the distorted grains essentially vanished and were replaced by fine recrystallized grains and subgrains. Indeed, these maps demonstrate the formation of recrystallized grains with ⟨101⟩//ND orientations, which are represented in green. Thus, the textures of the annealed specimens were achieved through the formation of new grains, which grew at the expense of the deformed microstructure resulting from oriented growth.

As shown in Figs. 6(j−l), small recrystallized crystal nuclei continued to grow through grain boundary migration after annealing for 420 min, generating recrystallized grains, and annealing twins were formed. For the CR specimens, grains with (or close to) a ⟨101⟩//ND orientation preferentially nucleated and grew with ongoing annealing, and fine recrystallized grains were formed, as shown in Figs. 6(f−l). The grain sizes of these annealed specimens demonstrate that the migration rates of the recrystallized grain boundaries with different orientations differed during annealing according to the rolling path applied to each specimen. Interestingly, RD-420 had the smallest grain size (8.7 μm). The results showed that the grain size decreased after rolling deformation and annealing, and the copper foil had higher strength, making it easier to perform subsequent rolling or drawing deformation, and reducing the risk of deformation instability.

The grain sizes of the RD, TD, and CR specimens annealed for 60 and 420 min are compared in Fig. 7. The average grain sizes of the RD-60, TD-60 and CR-60 specimens were 6.6, 8.0 and 8.6 μm, respectively, and increased to 8.7, 12.0, and 10.8 μm, respectively, after annealing for 420 min. This result is because the migration rates of the recrystallized grain boundaries with different orientations varied during annealing based on chosen rolling path. Furthermore, the recrystallized grain size of TD and CR was significantly larger than that of RD, because different rolling paths alter the deformation energy storage and grain boundary characteristics of the samples, influencing the migration rate of grain boundaries during the recrystallization process. For the RD samples, smaller grain boundaries were formed owing to lower migration rates, whereas for the TD and CR samples, grains with larger size were formed owning to higher migration rates.

The band contrast and boundary misorientation angles of the RD-60, TD-60, and CR-60 samples are shown in Fig. 8. The band contrast in Figs. 8(a, c, e) clearly reveals the recrystallized grains. The grain boundaries can be classified into low-angle grain boundaries (LAGBs) and high-angle

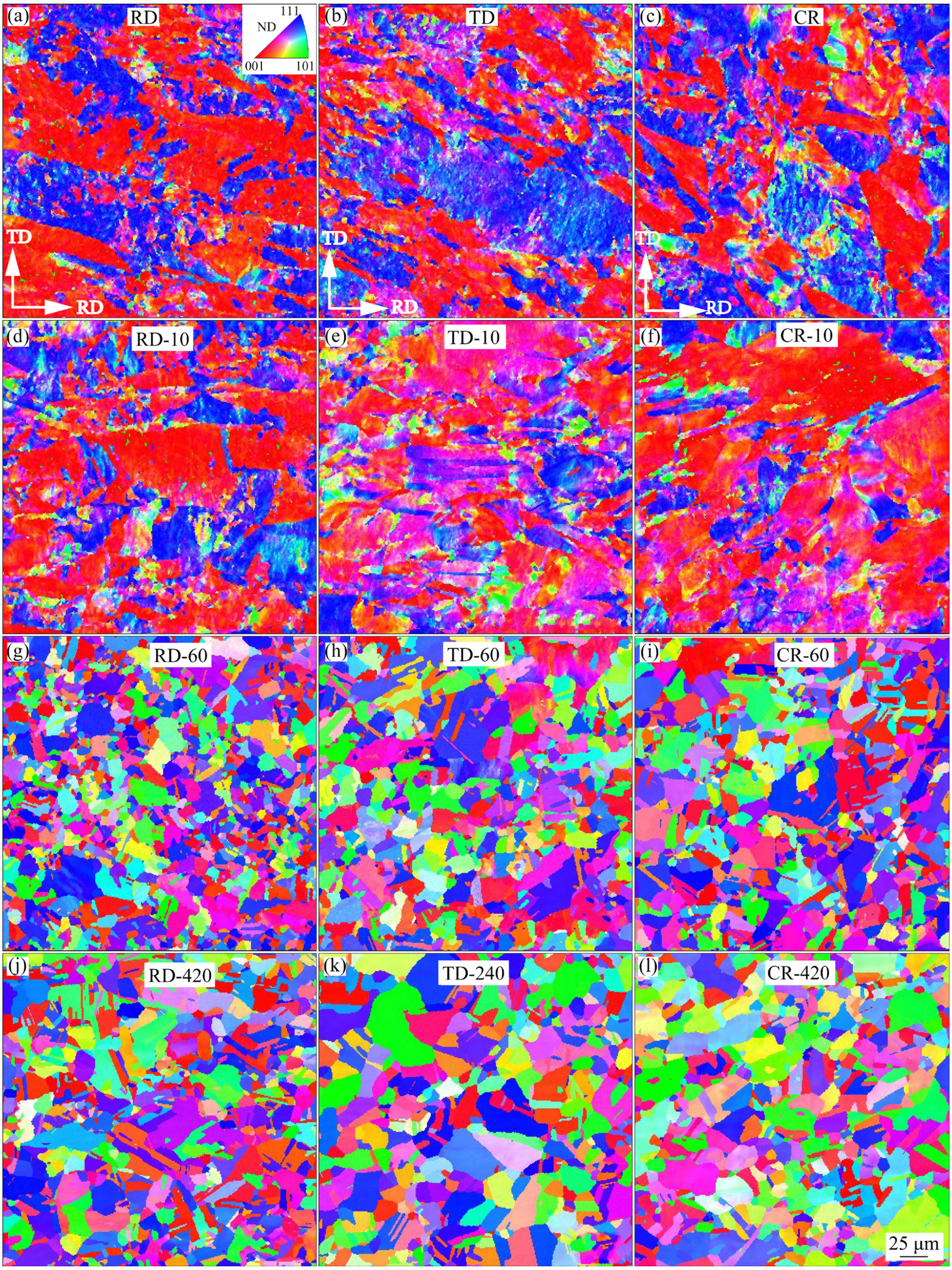

Fig. 6 EBSD orientation maps of specimens according to rolling path and annealing time: (a−c) Cold-rolled; (d−f) 400 °C, 10 min; (g−i) 400 °C, 60 min; (j−l) 400 °C, 420 min

grain boundaries (HAGBs) with the misorientations of 2°−15° and >15°, respectively. Figures 8(b, d, f) show pronounced HAGBs with fractions of 61.6%, 46.9%, and 89.1%, respectively. PAN et al [30] used a simple drawing process to introduce a large number of low-angle nanoscale dislocation boundaries into coarse-grained pure copper. This not only significantly improved tensile strength but also resulted in a fatigue limit of up to 130 MPa and a fatigue ratio of 0.35, representing a record for

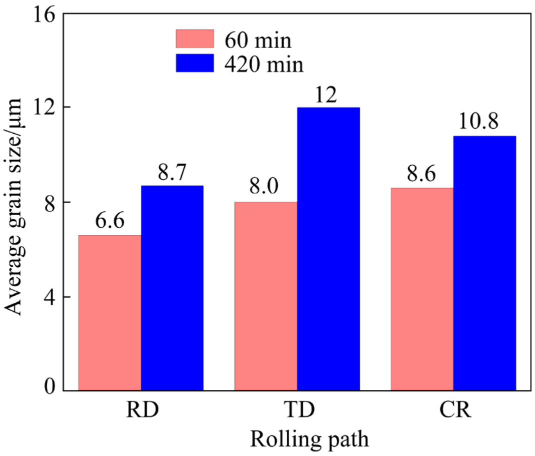

Fig. 7 Average grain sizes according to rolling path and annealing time

pure copper. The fractions of LAGBs for RD-60, TD-60, and CR-60 samples were 38.4%, 53.1% and 10.9%, respectively, which could improve the tensile strength of the samples. According to ZHAO et al [31], the etching performance of copper foil is steadily improved when the proportion of LAGBs decreases, owing to the low energy of these boundaries. The band contrast and boundary misorientation angles of the RD-420, TD-420, and CR-420 samples are shown in Fig. 9. Figures 9(a, c, e) show the recrystallized grains clearly. Figures 9(b, d, f) show pronounced HAGBs with fractions of 93.8%, 97.0%, and 95.4%, respectively. These results occurred because after annealing for 420 min, the nucleation and growth recrystallization processes were finished, resulting in the formation of HAGBs.

3.3 Texture evolution of cold-rolled pure Cu during annealing

The texture evolution of the Cu specimens during annealing after being subjected to different rolling paths was investigated using the pole figure (PF) results shown in Figs. 10−12. The textural evolutions from RD-10 to RD-60 and RD-420 are shown in Fig. 10. The cold-rolled RD specimen exhibited prominent {100}⟨100⟩ cubic texture and {111}⟨100⟩ texture, as illustrated in Fig. 10(a). After short-term annealing for 10 min, the textural composition did not change significantly, but the prominence of the cubic and Goss textures decreased. This is because short-term annealing reduced the dislocation density of specimen, relaxed the stress, and resulted in recovery and recrystallization in locations with high distortion

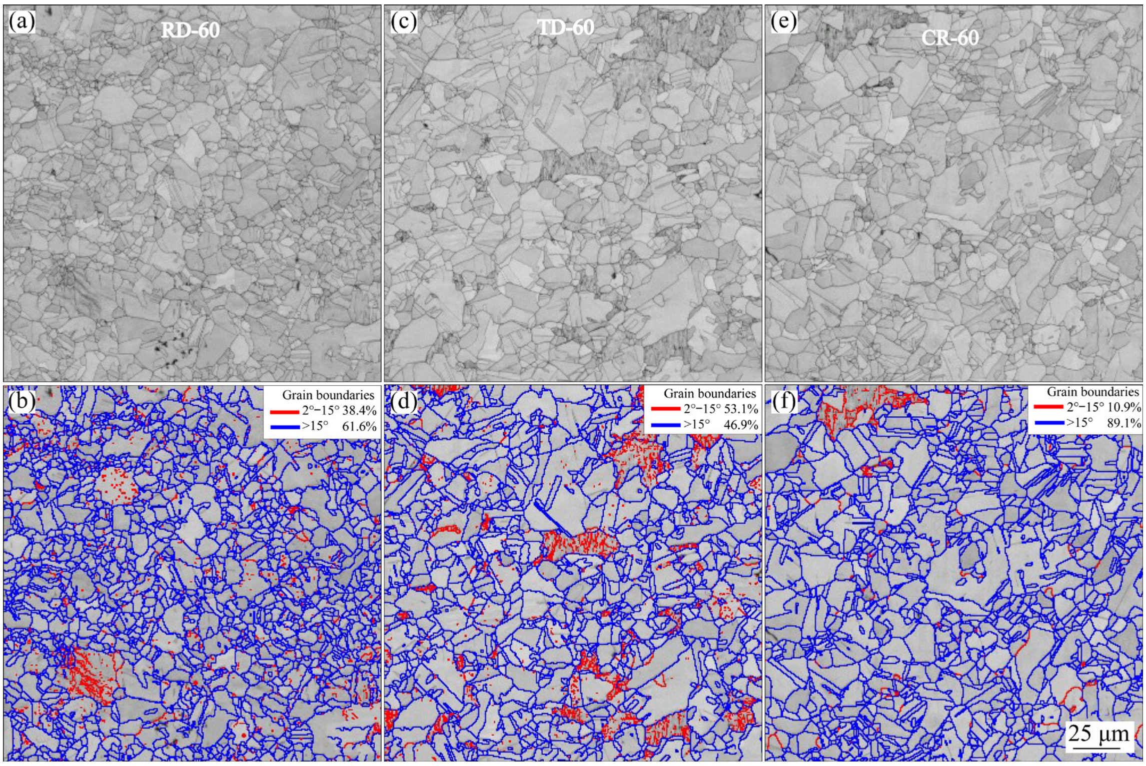

Fig. 8 Distributions of misorientation angles in RD-60, TD-60, and CR-60 specimens: (a, c, e) Band contrast; (b, d, f) Grain boundaries (Blue grain boundaries represent high-angle grain boundaries (>15°); red grain boundaries represent low-angle boundaries (2°−15°))

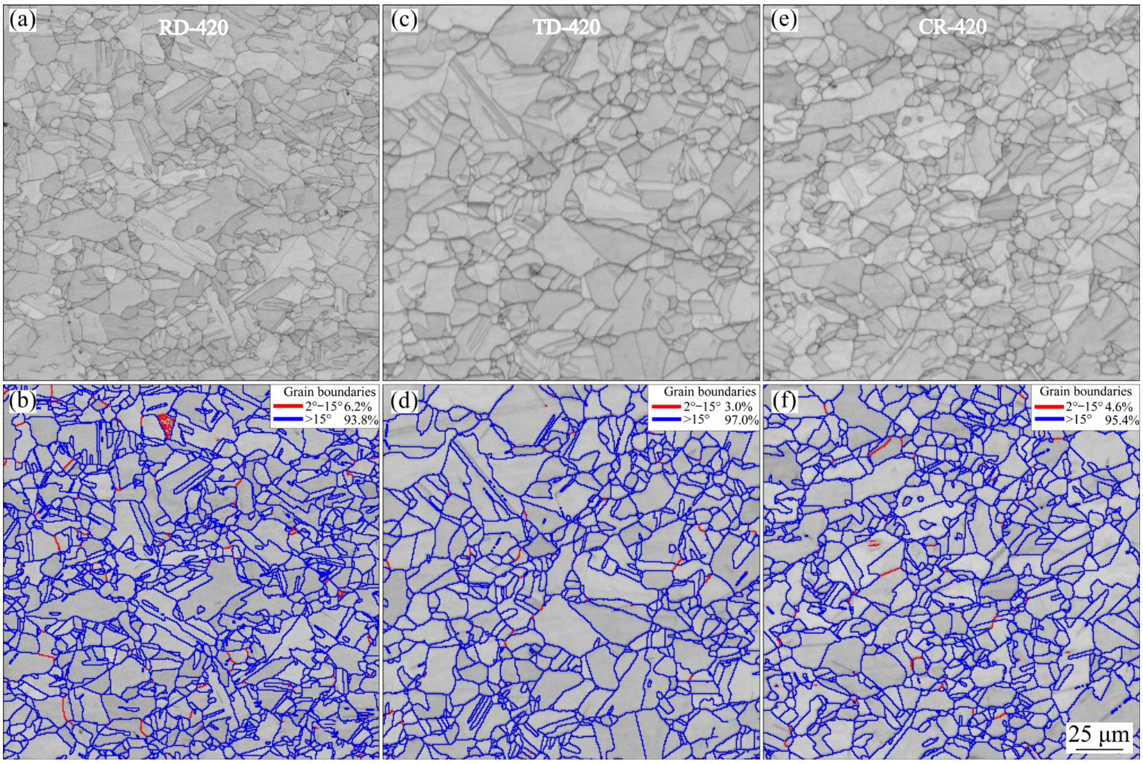

Fig. 9 Distributions of misorientation angles in RD-420, TD-420, and CR-420 specimens: (a, c, e) Band contrast; (b, d, f) Grain boundaries (Blue grain boundaries represent high-angle grain boundaries (>15°); red grain boundaries represent low-angle boundaries (2°−15°))

energy. Consequently, the textural composition remained unchanged, but its prominence decreased from 10.46 to 7.71. After annealing for 60 min, the PFs shown in Fig. 10(c) indicate that the prominence of the {100}⟨100⟩ cubic texture decreased to 3.56. As discussed above in relation to Fig. 6(g), the changes in the orientation maps of the specimens during annealing indicate that the deformation microstructure disappeared, forming small, recrystallized grains with different orientations and leading to the formation of random textures. Similarly, increasing the annealing time to 420 min, as shown in Fig. 10(d), resulted in the growth of grains with different orientations, leading to the appearance of random textures.

The PFs of the TD specimens annealed for different durations are shown in Fig. 11. According to standard PFs [32], the cold-rolled TD specimen exhibited a prominent {100}⟨100⟩ cubic texture, as well as {100}⟨111⟩ and {111}⟨120⟩ textures, as shown in Fig. 11(a). There was a slight change in the texture type after short-term annealing for 10 min; the analysis revealed that the prominence of the {100}⟨100⟩ cubic texture increased, whereas that of the {100}⟨111⟩ and {111}⟨120⟩ textures decreased slightly. The formation of recrystallized nuclei with different grain orientations during the annealing process, as well as the higher grain boundary migration rate of recrystallized nuclei with {100}⟨100⟩ orientations, resulted in the formation of larger recrystallized grains and more prominent {100}⟨100⟩ textures. After annealing for 60 min, the PFs shown in Fig. 11(c) indicate that the deformed texture basically vanished. The deformation grains disappeared and recrystallized grains with different orientations were formed. When the annealing time reached 420 min, as shown in Fig. 11(d), grains with different orientations grew, leading to the development of random textures.

The textural evolutions of the CR specimens during annealing are shown in Fig. 12. The cold-rolled CR specimen exhibited a prominent {100}⟨100⟩ cubic texture, as shown in Fig. 12(a), unlike the cold-rolled RD and TD specimens. After annealing for 10 min, the prominence of the {100}⟨100⟩ texture slightly increased, indicating that the recrystallized grains with {100}⟨100⟩

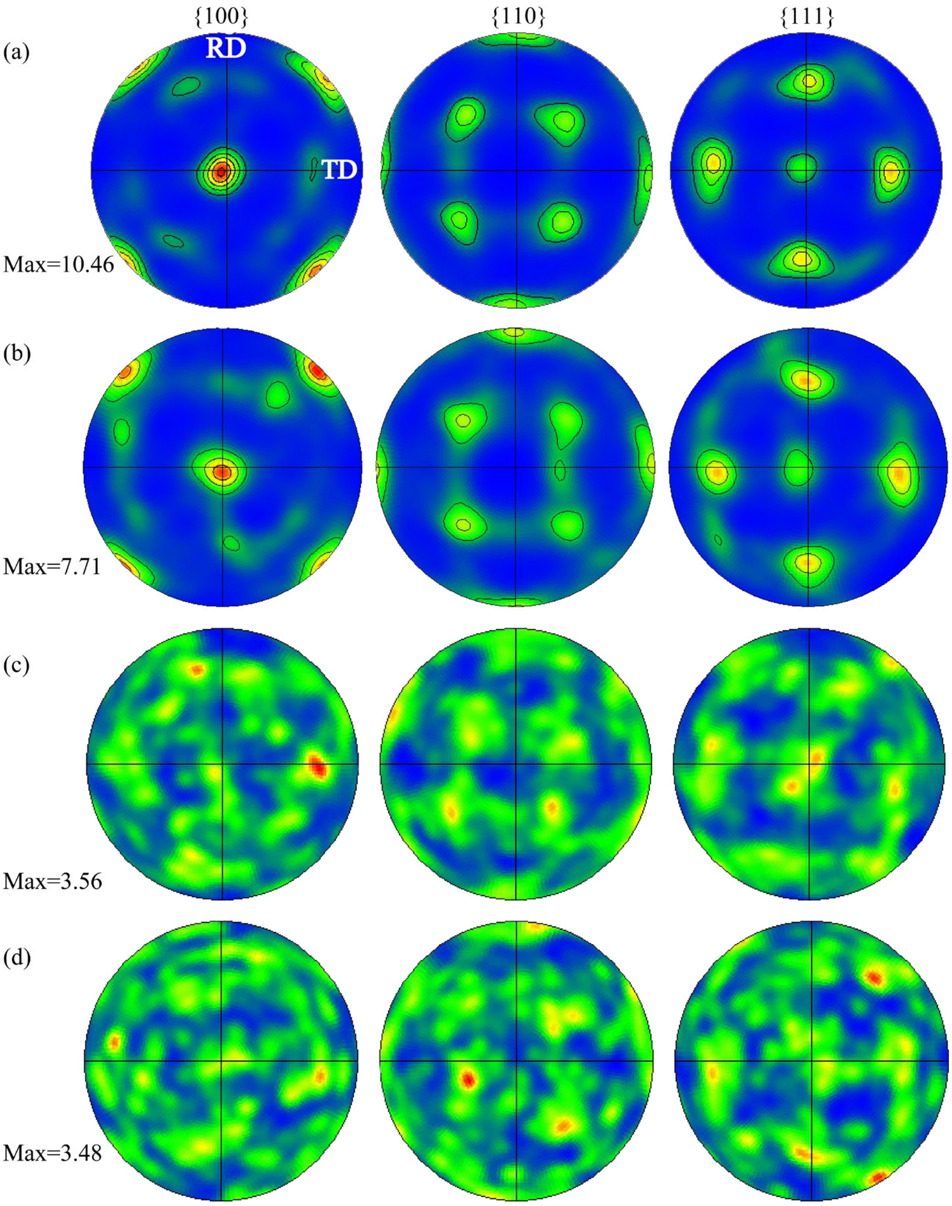

Fig. 10 Pole figures of RD samples during annealing: (a) Cold-rolled; (b) 10 min; (c) 60 min; (d) 420 min

orientation were formed during the annealing. However, the ⟨100⟩ orientation was deviated from the ND, as indicated in Fig. 12(b). After annealing for 60 min, the PFs shown in Fig. 12(c) indicate that {100}⟨100⟩ texture became less prominent, decreasing to 4.14 owing to the formation of grains with different orientations during recrystallization. When the annealing time reached 420 min, as shown in Fig. 12(d), grains with different grain orientations grew, leading to the development of random textures. PARDIS et al [33] studied the relationships among the microstructure, texture, and mechanical properties of commercial Cu over a wide strain range. Their results indicated that the ⟨111⟩ texture was predominant, whereas the ⟨100⟩ texture became significant only at extremely high strains. The textural evolution shows that the TP2 Cu has no evident preferred orientation after cold rolling and annealing. Moreover, YU et al [34] reported that pure Cu in the sintered state has no obvious preferred orientation.

3.4 Grain boundary characteristic distribution

Many studies have reported that low-Σ coincident site lattice (CSL) grain boundaries typically exhibit superior properties such as strength, fracture, and corrosion resistance compared to random HAGBs [18,27,28]. The low-Σ CSL (≤29) grain boundary results of RD-60, TD-60, and CR-60 are listed in Table 1. The fractions of

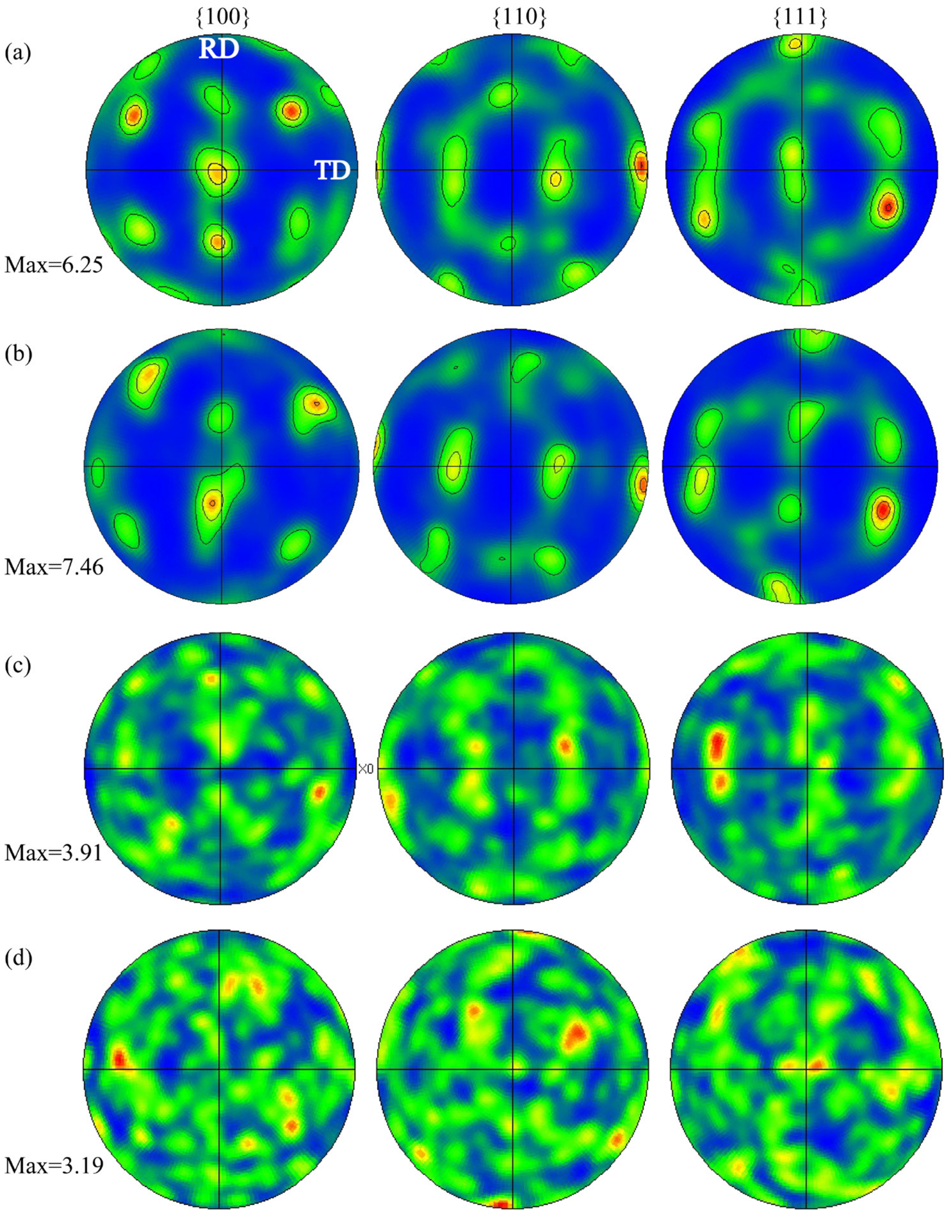

Fig. 11 Pole figures of TD samples during annealing: (a) Cold-rolled; (b) 10 min; (c) 60 min; (d) 420 min

low-Σ CSL for RD-60, TD-60, and CR-60 specimens were 31.5%, 26.7%, and 55.0%, respectively. The low-Σ CSL ($\Sigma\leq 29$) grain boundary distributions of RD-420, TD-420, and CR-420 are shown in Fig. 13. The types of special boundaries in the specimens were generally Σ3 CSL boundaries, as indicated by the red outlines, regardless of the applied rolling path. Only small quantities of Σ9 and Σ27 CSL boundaries were present, as represented by the purple and green outlines, respectively. Finally, the random HAGBs are represented by gray outlines. Additionally, Table 1 lists the GBCD results of the RD-420, TD-420, and CR-420 specimens. The low-Σ CSL grain boundary fractions for RD-420, TD-420, and CR-420 were 58.7%, 56.4%, and 56.3%, respectively. Although other boundaries, such as Σ9, arise for geometric reasons, the coherent Σ3 boundary is favorable in terms of energy considerations [23,35]. Twin-related domains are formed when two Σ3 CSLs that do not share an axis of rotation intersect to form a Σ9 CSL boundary. This boundary subsequently interacts with other Σ3 boundaries to form Σ27 or new Σ3 boundaries behind the migrating grain boundary front [27,36,37]. Several studies have indicated that a high $(\Sigma 9+\Sigma 27)/\Sigma 3$ ratio can interrupt the connectivity of the random HAGB network [27]. The corresponding ratios for RD-60, TD-60, and CR-60 were 0.14, 0.15, and 0.12, respectively. In contrast, the ratios for RD-420,

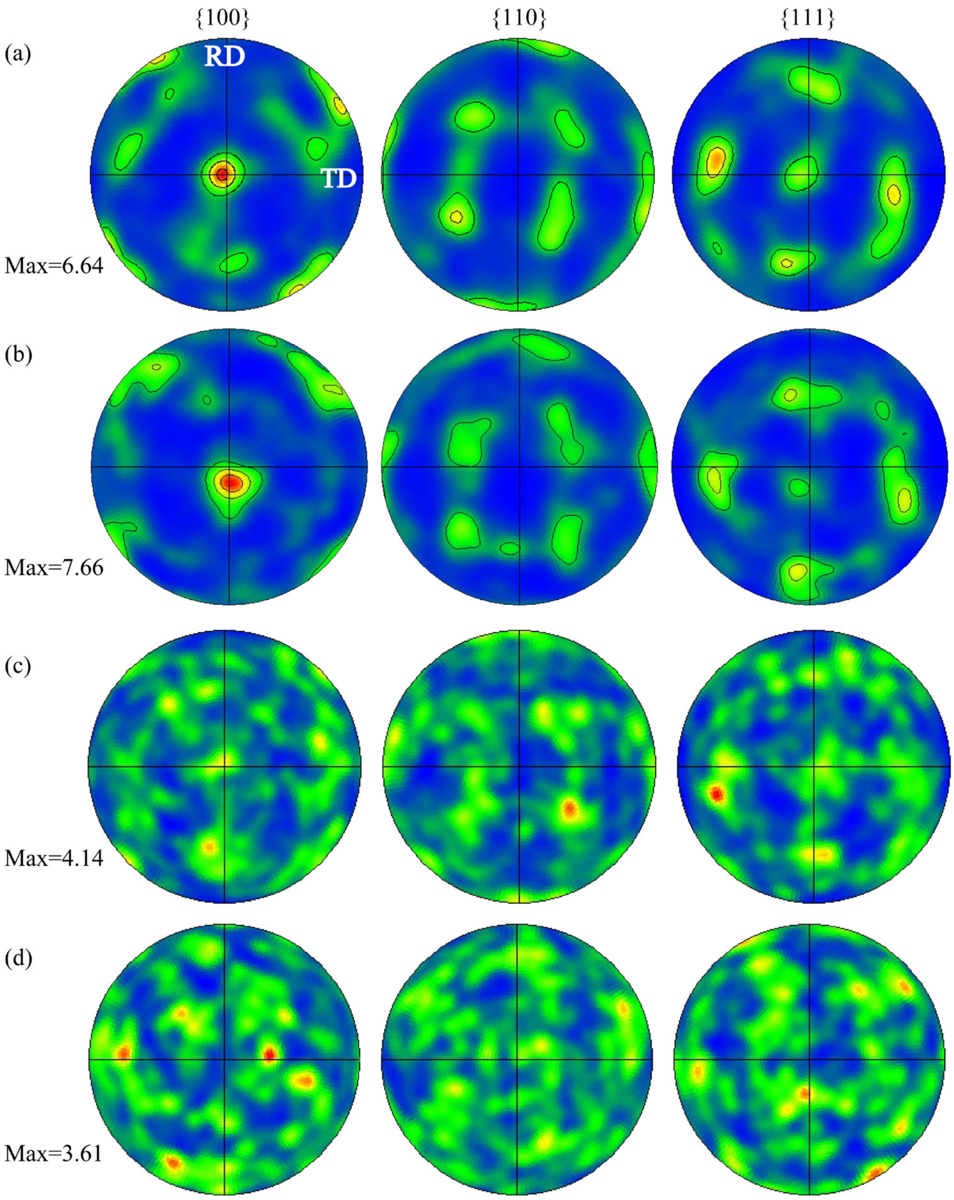

Fig. 12 Pole figures of CR samples during annealing: (a) Cold-rolled; (b) 10 min; (c) 60 min; (d) 420 min

Table 1 GBCDs of samples annealed for 60 and 420 min

Sample	Low-Σ CSL boundary/%	Σ3/%	(Σ9+Σ27)/%	(Σ9+Σ27)/Σ3
RD-60	31.5	27.6	3.9	0.14
TD-60	26.7	23.3	3.4	0.15
CR-60	55.0	49.1	5.9	0.12
RD-420	58.7	51.8	6.9	0.13
TD-420	56.4	50.2	6.2	0.12
CR-420	56.3	49.5	6.8	0.14

TD-420, and CR-420 were 0.13, 0.12, and 0.14, respectively. For the RD and TD specimens, the low-Σ CSL fraction increased with increasing the annealing time and the (Σ9+Σ27)/Σ3 ratio decreased, whereas for the CR specimen, the ratio increased. According to GUAN et al [38], a grain boundary engineering treatment based on dynamic recrystallization can simultaneously enhance the high-temperature strength and ductility of face-centered cubic metals. In terms of tensile performance, YOU et al [27] reported the strength and ductility of the grain-boundary engineered high-entropy specimens by this treatment. They pointed out that optimizing the GBCD has various effects on the deformation mechanism, such as enhancing strain uniformity through low-Σ CSL grain boundaries and improving the dislocation proliferation and stress cracking resistance.

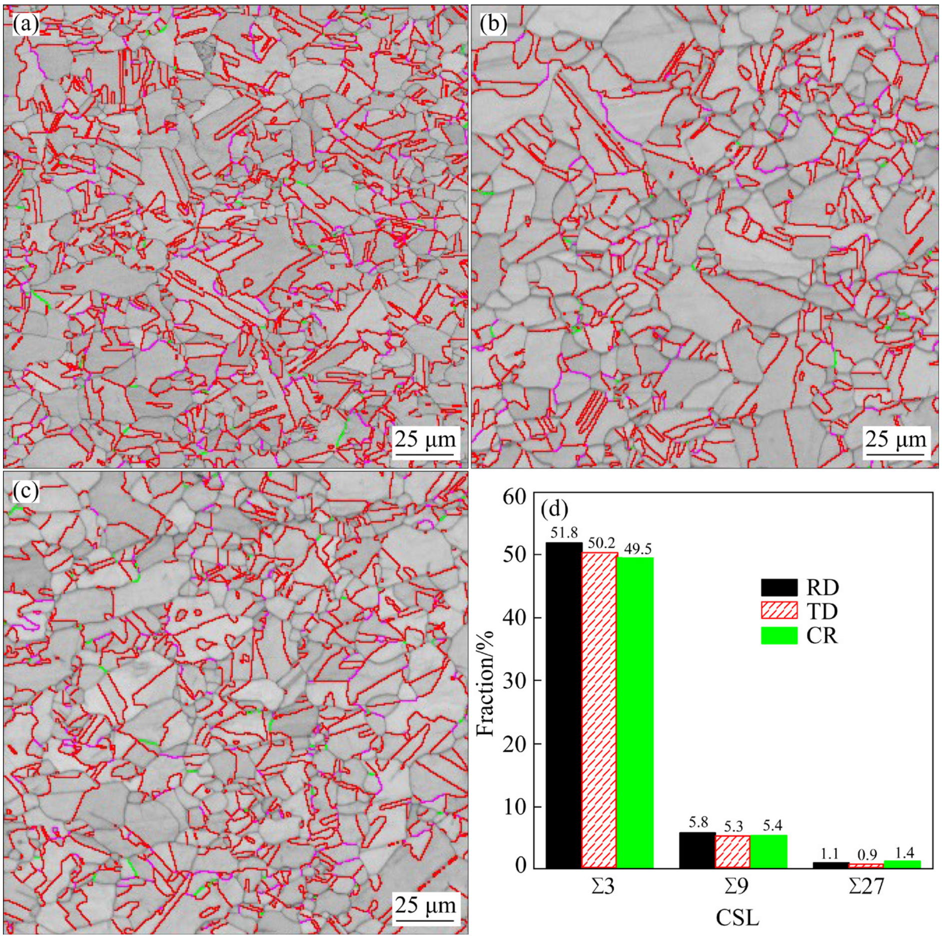

Fig. 13 Low-Σ CSL boundary distributions in RD-420 (a), TD-420 (b), and CR-420 (c) specimens (Σ3, Σ9, and Σ27 are indicated in red, purple, and green, respectively); Distribution of CSL boundaries according to different specimens (d)

3.5 Tensile property evolution of annealed specimens

The tensile tests were performed at room temperature to evaluate the mechanical properties of the Cu sheets according to the applied rolling path and annealing time. Figure 14 shows the evolution of the tensile stress–strain curves of the specimens. The yield strength, ultimate strength and elongation of the specimens are listed in Table 2.

After annealing for 10 min, all specimens exhibited relatively high strength but low ductility. The yield strengths of the different specimens varied slightly. Their ultimate strengths were 375, 360, and 346 MPa for RD-10, CR-10, and TD-10, respectively. As illustrated in Figs. 6(d, e, f), several deformed structures remained in the specimens, resulting in relatively high dislocation densities and substructures. This provided significant resistance against dislocation slip during tensile deformation.

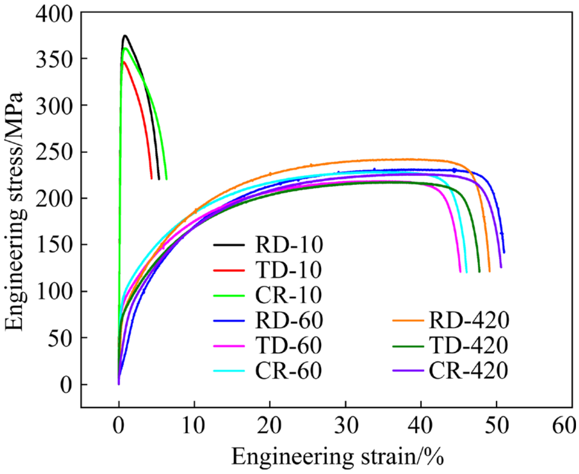

Fig. 14 Engineering stress–strain curves of specimens

After annealing for 60 min, the ultimate strengths of the specimens were 230, 228, and 214 MPa for RD-60, CR-60, and TD-60 samples, respectively. As discussed in Fig. 6, the distorted grains essentially vanished and were replaced by recrystallized grains. The yield strengths for the RD-60, TD-60, and CR-60 specimens were 81, 81 and 88 MPa, respectively. The corresponding elongation values were 49%, 43%, and 45%, respectively. Different rolling paths altered the deformation energy storage and GBCD of cold-rolled copper, and as a result, the recrystallized samples had slightly different mechanical properties. After annealing for 420 min, the ultimate strengths of the specimens were 240, 225, and 216 MPa for RD-420, CR-420, and TD-420, respectively, and their yield strengths were 69, 77, and 66 MPa, respectively.

As the annealing time increased, the yield strength decreased. After the annealing time was extended from 60 to 420 min, the yield strength of RD sample decreased from 81 to 69 MPa, with reduction of ~15%. This is because the grain size increased from 6.6 to 8.7 μm, the number of grain boundaries decreased, the hindering effect on dislocation movement was weakened, and the plastic deformation resistance of the RD-420 sample decreased. As discussed in Section 3.4, strain uniformity can be enhanced by low-Σ CSL grain boundaries, which improves the dislocation increment and stress cracking resistance. The low-Σ CSL grain boundary proportion for the RD-420 sample was 58.7%. The grain growth reduced the plastic deformation resistance of the TP2 copper, while the low-Σ CSL grain boundaries improved its tensile strength. Together, these effects slightly increased the ultimate strength of the RD-420 specimen, from 230 to 240 MPa, along with a decrease in elongation.

For the TD samples, the grain size increased from 8.0 to 12.0 μm with increasing the annealing time from 60 to 420 min. The low-Σ CSL grain boundary fraction in the TD-420 sample was 56.4%. The combined effect of the grain size and low-Σ CSL grain boundary fraction slightly increased the ultimate tensile strength of the TD-420 sample, from 214 to 216 MPa. However, the ultimate tensile strength of the CR-420 sample slightly decreased, from 228 to 225 MPa, and the elongation slightly increased. This might be related to the low-Σ CSL grain boundaries, as the fractions of these boundaries for CR-60 and CR-420 were 55.0% and 56.3%, respectively. The grain size affects the ultimate tensile strength to a greater extent compared to low-Σ CSL grain boundaries, resulting in a slight decrease in tensile strength. By comparing the mechanical properties of cold-rolled copper with different rolling paths after annealing, as listed in Table 2, RD-60 exhibited suitable mechanical properties and the highest plasticity among the samples, with yield strength, ultimate tensile strength, and elongation of 81 MPa, 230 MPa, and 49%, respectively. Similarly, AFIFEH et al [39] reported that after the annealing, asymmetrically cold-rolled pure Cu at 200 °C for 60 min, its ultimate tensile strength and elongation were 229.9 MPa and 32%, respectively.

Table 2 Mechanical properties achieved by different rolling paths after annealing at 400 °C for different durations

Sample	Yield strength/ MPa	Ultimate tensile strength/MPa	Elongation/ %
RD-10	366	375	−
TD-10	340	346	−
CR-10	351	360	−
RD-60	81	230	49.0
TD-60	81	214	43.0
CR-60	88	228	45.0
RD-420	69	240	47.0
TD-420	66	216	45.0
CR-420	77	225	48.0

3.6 Fracture morphology

Figure 15 shows the SEM images of fracture surfaces on the annealed specimen after tensile testing. The specimens subjected to the annealing for 60 min exhibited the fracture morphologies comprising ductile fractures with numerous shallow dimples and fewer deep dimples. RD-60, TD-60, and CR-60 samples exhibited elongations of 49.0%, 43.0%, and 45.0%, respectively, indicating remarkable ductility. After annealing for 420 min, the fracture morphologies of the specimens exhibited the same variation pattern, with a considerable number of ductile dimples reflecting ductile fracture. The elongations of the RD-420, TD-420, and CR-420 specimens were 47%, 45%, and 48%, respectively, indicating high ductility.

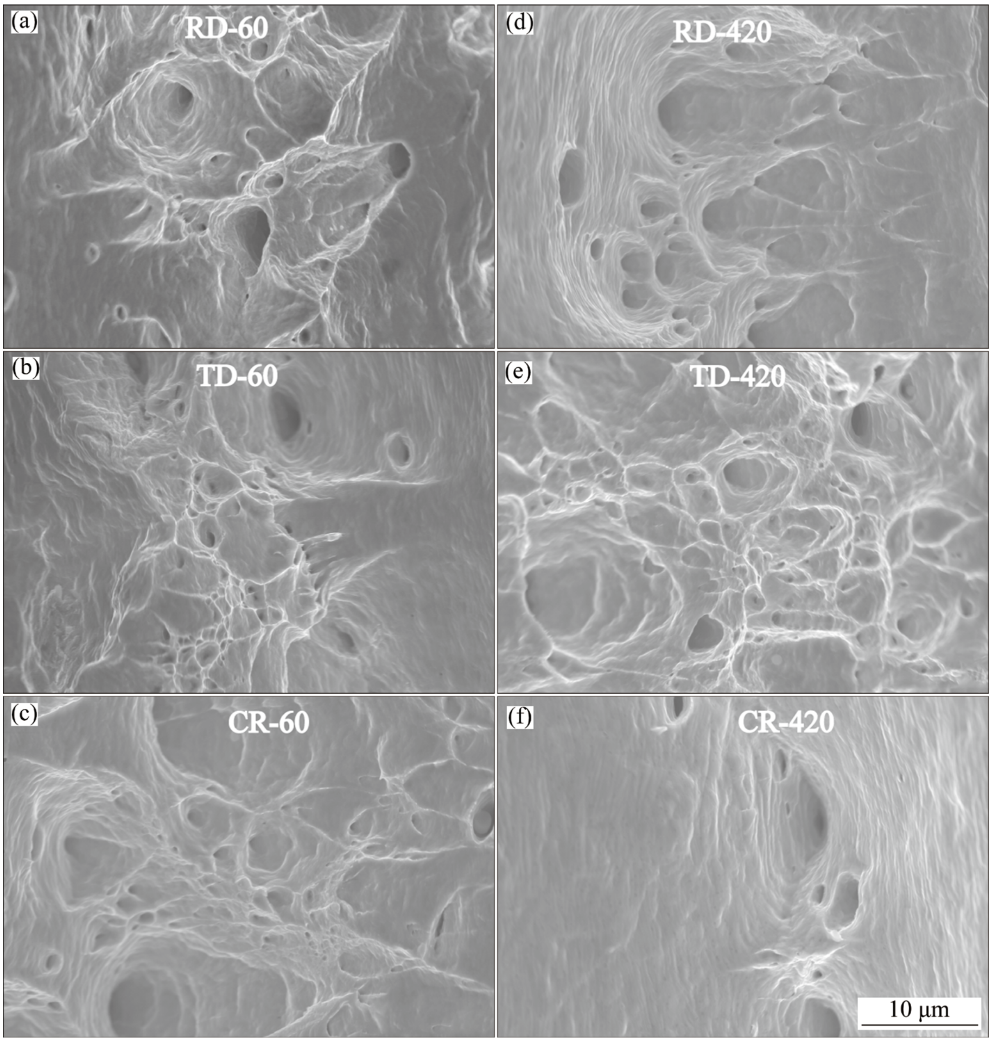

Fig. 15 Tensile fracture morphologies of annealed specimens: (a) RD-60; (b) TD-60; (c) CR-60; (d) RD-420; (e) TD-420; (f) CR-420

4 Conclusions

(1) Different rolling paths changed the grain boundary orientation of cold-rolled copper, causing recrystallized grains to nucleate and grow in an oriented manner. The RD, TD, and CR specimens recrystallized after annealing at 400 °C for 60 min.

(2) The unannealed cold-rolled specimens exhibited intensive $\{100\}\langle 100\rangle$ cubic and $\{011\}\langle 100\rangle$ Goss textures. The evolution of these textures indicated that cold-rolled copper with different rolling paths did not show an obvious preferred orientation after annealing and random textures were formed.

(3) The migration rates of the recrystallized grain with different orientations varies during annealing based on the rolling path applied. The RD-60 specimen exhibited the smallest grain size (6.6 μm).

(4) The combination of an appropriate grain size and the low-Σ CSL grain boundaries provided the RD-60 samples with appropriate mechanical properties and the highest plasticity. The yield strength, ultimate tensile strength, and elongation of the RD-60 sample were 81 MPa, 230 MPa, and 49%, respectively. These findings can guide the design of further deformation treatments, such as rolling and drawing, and facilitate the preparation of thinner rolled copper foils to improve the performance of pure copper foil components in electronic devices.

CRediT authorship contribution statement

Jing CHEN: Conceptualization, Methodology, Formal analysis, Investigation, Writing − Original draft, Writing − Review & editing; **Wen-jie XU:** Data curation; **Jia-hao YANG:** Investigation; **Zhi YANG:** Data curation; **Hong-li SHI:** Formal analysis; **Gao-yong LIN:** Formal analysis, Supervision; **Zhu-min LI:** Methodology, Supervision; **Xu SHEN:** Investigation; **Bo JIANG:** Validation; **Hui-qun LIU:** Supervision, Writing − Review & editing; **Kai-xuan GUI:** Methodology.

Declaration of competing interest

The authors declare that they have no known competing financial interests or personal relationships that could have appeared to influence the work reported in this paper.

Acknowledgments

This work was financially supported by the National Natural Science Foundation of China (No. 52201099), the Scientific Research Starting Foundation of Anhui Polytechnic University, China (No. S022021004), the Open Research Fund of Anhui Key Laboratory of High-Performance Non-ferrous Metal Materials, China (No. YSJS-2023-1), Undergraduate Scientific Research Project of Anhui Polytechnic University, China, and School Level Scientific Research Project of Anhui Polytechnic University, China (No. Xjky2022028).

References

[1] QIN Liu-xin, ZHOU Tao, JIANG Xiao-yu, WANG Meng, HU Jin-hui, WU Zi-xiao, MENG Xiang-peng, JIANG Yan-bin, LI Zhou. Microstructure and properties of Cu−Ni−Co−Si−Cr−Mg alloy by multistage thermomechanical treatment [J]. Transactions of Nonferrous Metals Society of China, 2023, 33: 3739−3755. https://doi.org/10.1016/S1003-6326(23)66367-8.

[2] YANG Y, ZHANG X X, LI M X, LI R G, MIAO K S, LI X W, LIU C L, WU H, FAN G H. Effects of intermediate aging on the microstructure, strength and texture evolution of the Cu−Cr− Zr−Hf alloys [J]. Materials Science and Engineering A, 2024, 899: 146479. https://doi.org/10.1016/j.msea.2024.146479.

[3] WANG Xu, LI Zhou, XIAO Zhu, QIU Wen-ting. Microstructure evolution and hot deformation behavior of Cu−3Ti−0.1Zr alloy with ultra-high strength [J]. Transactions of Nonferrous Metals Society of China, 2020, 30: 2737−2748. https://doi.org/10.1016/S1003-6326(20)65416-4.

[4] MA M Z, XIAO Z, MENG X P, LI Z, GONG S, DAI J, JIANG H Y, JIANG Y B, LEI Q, WEI H G. Effects of trace calcium and strontium on microstructure and properties of Cu−Cr alloys [J]. Journal of Materials Science and Technology, 2022, 112: 11−23. https://doi.org/10.1016/j.jmst.2021.08.080.

[5] LIU Ding-kai, HUANG Guang-sheng, GONG Gui-lin, WANG Guan-gang, PAN Fu-sheng. Influence of different rolling routes on mechanical anisotropy and formability of commercially pure titanium sheet [J]. Transactions of Nonferrous Metals Society of China, 2017, 27: 1306−1312. https://doi.org/10.1016/S1003-6326(17)60151-1.

[6] ZHOU Shuang, YANG Yi-hai, LEI Qian, CHEN Ru-xuan, GONG Shen. Effect of fabrication methods on the microstructure and properties of a Cu−Cr−Nb alloy [J]. Materials Science and Engineering A, 2022, 858: 144159. https://doi.org/10.1016/j.msea.2022.144159.

[7] XIN Zhao, JIANG Yan-bin, WU Zi-xiao, TAN Fei, QIU Wen-ting, LI Jia-hao, XIA Zhuo-ran, DAI Wen, LI Lin-han, XIAO Zhu. Effect of cryogenic rolling and multistage thermomechanical treatment on the microstructure and properties of the Cu−0.4Cr−0.39Zn−0.1Mg−0.07Zr alloy [J]. Materials Characterization, 2024, 207: 113557. https://doi.org/10.1016/ j.matchar.2023.113557.

[8] SHI H L, GAN W M, ESLING C, ZHANG Y D, WANG X J, MAAWAD E, STARK A, LI X H, WANG L D. Recrystallization texture evolution of cold-rolled Cu foils governed by microstructural and sample geometrical factors during heating [J]. Materials Characterization, 2023, 196: 112605. https://doi.org/10.1016/j.matchar.2022.112605.

[9] LI J W, DING C G, CHEN W J, SHAN D B, GUO B, XU J. Strain localization and ductile fracture mechanism of micro/mesoscale deformation in ultrafine-grained pure copper [J]. Materials & Design, 2023, 229: 111873. https://doi.org/10.1016/ j.matdes.2023.111873.

[10] GU C F, HOFFMAN M, TOTH L S, ZHANG Y D. Grain size dependent texture evolution in severely rolled pure copper [J]. Materials Characterization, 2015, 101: 180−188. https://doi.org/10.1016/j.matchar.2015.02.003.

[11] MA Ru, LU Yue, WANG Ling, WANG Yi-nong. Influence of rolling route on microstructure and mechanical properties of AZ31 magnesium alloy during asymmetric reduction rolling [J]. Transactions of Nonferrous Metals Society of China, 2018, 28: 902−911. https://doi.org/10.1016/S1003-6326(18)64724-7.

[12] ZHANG Tao, HOU Yu-zhu, QUE Biao-hua, TIAN Yu-xin, CHEN Liang. Combining pre-rolling with retrogression and re-aging treatment to balance strength and corrosion resistance of 7A99 Al alloy [J]. Transactions of Nonferrous Metals Society of China, 2023 33: 2913−2925. https://doi.org/10.1016/S1003-6326(23)66307-1.

[13] LIU Zhan, NIE Jin-feng, ZHAO Yong-hao. Effect of deformation processing on microstructure evolution and mechanical properties of Mg−Li alloys: A review [J]. Transactions of Nonferrous Metals Society of China, 2024, 34: 1−25. https://doi.org/10.1016/S1003-6326 (23)66379-4.

[14] ZHAO S, WANG Y, PENG L, ZHANG Y X, RAN R, YUAN G. Effect of annealing temperature on microstructure and mechanical properties of cold-rolled commercially pure titanium sheets [J]. Transactions of Nonferrous Metals Society of China, 2020, 32: 2587−2597. https://doi.org/10.1016/S1003-6326(22)65968-5.

[15] ZHANG M X, DENG L P, WANG B S, XIANG H L. Effect of torsional rate on the gradient microstructure, texture evolutions and microhardness of pure copper [J]. Materials Characterization, 2020, 161: 110141. https://doi.org/10.1016/j.matchar.2020.110141.

[16] GUPTA A, YOO T H, KAUSHIK L, LEE J W, KIM Y K, CHOI S H. Unveiling the room-temperature softening phenomenon and texture evolution in room-temperature- and cryogenic-rolled ETP copper [J]. International Journal of Plasticity, 2022, 156: 103340. https://doi.org/10.1016/j.ijplas.2022.103340.

[17] LI J K, REN X P, LING Z, WANG H B. Improving bending property of copper foil by the combination of double-rolling and cross rolling [J]. Journal of Materials Research and Technology, 2020, 9: 6922−6927. https://doi.org/10.1016/j.jmrt.2020.02.004.

[18] LI Jing-kun, REN Xue-ping, ZHANG Yan-ling, HOU Hong-liang, YAN Q. Microstructural response of copper foil to a novel double-cross rolling process [J]. Journal of Materials Research and Technology, 2020, 9: 15153−15163. https://doi.org/10.1016/j.jmrt.2020.11.003.

[19] DENG C, LIU S F, JI J L, HAO X B, ZHANG Z Q, LIU Q. Texture evolution of high purity tantalum under different rolling paths [J]. Journal of Materials Processing Technology, 2014, 214: 462−469. https://doi.org/10.1016/j.jmatprotec.2013.09.026.

[20] OERTEL C G, HÜNSCHE I, SKROTZKI W, LORICH A, KNABL W, RESCH J, TRENKWALDER T. Influence of cross rolling and heat treatment on texture and forming properties of molybdenum sheets [J]. International Journal of Refractory Metals and Hard Materials, 2010, 28: 722−727. https://doi.org/10.1016/j.ijrmhm.2010.07.003.

[21] XU J, GUAN B, FU R, WU Y, HU Q, ZOU J, HUANG G J, YAN C J. Tailoring the microstructure and mechanical properties of Cu−Fe alloy by varying the rolling path and rolling temperature [J]. Journal of Materials Research and Technology, 2023, 27: 182−193. https://doi.org/10.1016/j.jmrt.2023.09.273.

[22] XU J, PENG Y S, GUAN B, XIN Y C, CHAPUIS A, HUANG G J, LIU Q. Tailoring the microstructure and texture of a dual-phase Mg−8Li alloy by varying the rolling path [J]. Materials Science and Engineering A, 2022, 844: 143202. https://doi.org/10.1016/j.msea.2022.143202.

[23] YANG X Y, WANG P, HUANG M. Grain boundary evolution during low-strain grain boundary engineering achieved by strain-induced boundary migration in pure copper [J]. Materials Science and Engineering A, 2022, 833: 142532. https://doi.org/10.1016/j.msea.2021.142532.

[24] LIU B, DING Y T, XU J Y, WANG X M, GAO Y B, HU Y, CHEN D L. Achievement of grain boundary engineering by transforming residual stress in selective laser-melted Inconel 718 superalloy [J]. Materials Science and Engineering A, 2023, 866: 144683. https://doi.org/10.1016/j.msea.2023.144683.

[25] GAO S B, HU Z H, DUCHAMP M, KRISHNAN RAMA KRISHNAN P S, TEKUMALLA S, SONG X, SEITA M. Recrystallization- based grain boundary engineering of 316L stainless steel produced via selective laser melting [J]. Acta Materialia, 2020, 200: 366−377. https://doi.org/10.1016/j.actamat.2020. 09.015.

[26] ZHU Y L, CAO Y, MA J H, ZHANG J K, HE Q B, LUO R, JIA X H, LIU Q Y, XIAO J. Cryogenic deformation tailors the dislocation accumulation mode to modify grain boundary character distribution of Incoloy 925 [J]. Materials Characterization, 2023, 202: 112995. https://doi.org/10.1016/j.matchar.2023.112995.

[27] YOU Z Y, TANG Z Y, LI J P, CHU F B, DING H, MISRA R D K. Effect of grain boundary engineering on grain boundary character distribution and deformation behavior of a TRIP-assisted high-entropy alloy [J]. Materials Characterization, 2023, 205. https://doi.org/10.1016/j. matchar.2023.113294.

[28] GUAN X J, SHI F, JI H M, LI X W. Gain boundary character distribution optimization of Cu−16at.%Al alloy by thermomechanical process: Critical role of deformation microstructure [J]. Materials Science and Engineering A, 2019, 765: 138299. https://doi.org/10.1016/j.msea.2019.138299.

[29] LEE J, JEONG H, PARK S. Effect of extrusion ratios on microstructural evolution, textural evolution, and grain boundary character distributions of pure copper tubes during hydrostatic extrusion [J]. Materials Characterization, 2019, 158: 109941. https://doi.org/10.1016/j.matchar.2019.109941.

[30] PAN Q S, JING L J, LU L. Enhanced fatigue endurance limit of Cu through low-angle dislocation boundary [J]. Acta Materialia, 2023, 244: 118542. https://doi.org/10.1016/j.actamat.2022.118542.

[31] ZHAO W C, FENG R, WANG X W, FENG M, SUN Y M, GONG B K, HAN X J, FENG T J. Relationship between microstructure and etching performance of 12 μm thick rolled copper foil [J]. Journal of Materials Research and Technology, 2022, 21: 1666−1681. https://doi.org/10.1016/j.jmrt.2022.10.009.

[32] GU C F, TOTH L S, ZHANG Y D, HOFFMAN M. Unexpected brass-type texture in rolling of ultrafine-grained copper [J]. Scripta Materialia, 2014, 92: 51−54. https://doi.org/10.1016/j.scriptamat.2014.08.012.

[33] PARDIS N, CHEN C, EBRAHIMI R, TOTH L S, GU C F, BEAUSIR B, KOMMEL L. Microstructure, texture and mechanical properties of cyclic expansion−extrusion deformed pure copper [J]. Materials Science and Engineering A, 2015, 628: 423−432. https://doi.org/10.1016/j.msea.2015.01.003.

[34] YU J N, WANG L D, GUAN Y K, SHAO B, LIU Z Y, ZONG Y Y. A high strength and high electrical conductivity graphene/Cu composite with good high-temperature stability [J]. Materials Characterization, 2023, 201: 112928. https://doi.org/10. 1016/j.matchar.2023.112928.

[35] QUAN S Y, SONG R B, SU S R, HUANG Y, CAI C H, WANG Y J, WANG K K. Grain boundary engineering prepared by iterative thermomechanical processing of nickel-saving austenitic stainless steel: Excellent corrosion resistance and mechanical properties [J]. Materials Characterization, 2023, 196: 112601. https://doi.org/10.1016/j.matchar.2022.112601.

[36] ZHANG X H, XIONG D B, LIU Y Z, JIA Y L, ZHANG Y, ZHOU M, LIU H J, GENG Y F, WANG X Y, LIU P, SONG X G, ZHANG D. Multilayer graphene interface enabled ultrahigh extensibility for high performance bulk nanostructured copper [J]. Acta Materialia, 2024, 267: 119710. https://doi.org/10.1016/j. actamat.2024.119710.

[37] LAPEIRE L, SIDOR J, VERLEYSEN P, VERBEKEN K, DE GRAEVE I, TERRYN H, KESTENS L A I. Texture comparison between room temperature rolled and

cryogenically rolled pure copper [J]. Acta Materialia, 2015, 95: 224−235. https://doi.org/10.1016/j.actamat.2015.05.035.

[38] GUAN X J, SHI F, JI H M, LI X W. A possibility to synchronously improve the high-temperature strength and ductility in face-centered cubic metals through grain boundary engineering [J]. Scripta Materialia, 2020, 187: 216−220. https://doi.org/10.1016/j.scriptamat.2020.06.026.

[39] AFIFEH M, HOSSEINIPOUR S J, JAMAATI R. Effect of post-annealing on the microstructure and mechanical properties of nanostructured copper [J]. Materials Science and Engineering A, 2021, 802: 140666. https://doi.org/10.1016/j.msea.2020.140666.

冷轧路径对纯铜在退火过程中再结晶行为和力学性能的影响

陈　静 1,2,3，徐文杰 1,2，杨家豪 1,2，杨　志 1，石红利 1,2，
林高用 3，利助民 1,2，沈　旭 4，姜　波 5，刘会群 3，桂凯旋 1,2

1. 安徽工程大学 材料科学与工程学院，芜湖 241000；
2. 安徽工程大学 高性能有色金属材料安徽省重点实验室，芜湖 241000；
3. 中南大学 材料科学与工程学院，长沙 410083；
4. 中国科学院 等离子体物理研究所，合肥 230031；
5. 常州大学 材料科学与工程学院，常州 213164

摘　要：研究了不同冷轧路径的纯铜在 400 ℃退火 10、30、60 和 420 min 过程中的再结晶行为、晶界特征分布以及力学性能。不同的轧制路径改变了冷轧铜的晶界取向，导致再结晶晶粒定向成核和长大；而织构演变表明，不同轧制路径的冷轧铜在退火后没有表现出明显的择优取向。RD-60 样品的晶粒尺寸最小(6.6 μm)。结果表明，在晶粒尺寸和低∑CSL 晶界共同作用下，RD-60 样品具有较好的力学特性和高塑性，其屈服强度、极限抗拉强度和伸长率分别为 81 MPa、230 MPa 和 49%。这些结果可以为调整纯铜箔的微观结构和性能，以及通过轧制和拉拔等工艺设计为纯铜箔的制造路线提供指导。

关键词：轧制路径；晶界特征分布；纯铜；力学性能

(Edited by Bing YANG)